Effect of B and Fe substitution on structure of AB₃-type Co-free hydrogen storage alloy

WU Feng(吴 锋)[1, 2], ZHANG Min-yu(张旻昱)[1], MU Dao-bin(穆道斌)[1, 2]

1. Beijing Key Laboratory of Environmental Science and Engineering,
School of Chemical Engineering and Environment, Beijing Institute of Technology, Beijing 100081, China;
2. National Development Center of Hi-Tech Green Materials, Beijing 100081, China

Abstract: A series of hydrogen storage Co-free AB₃-type alloys were directly synthesized with vacuum mid-frequency melting method, within which Ni of $La_{0.7}Mg_{0.3}Ni_3$ alloy was substituted by Fe, B and (FeB) alloy, respectively. Alloys were characterized by XRD, EDS and SEM to investigate the effects of B and Fe substitution for Ni on material structure. The content of $LaMg_2Ni_9$ phase within $La_{0.7}Mg_{0.3}Ni_3$ alloy reaches 37.9% and that of $La_{0.7}Mg_{0.3}Ni_{2.9}(FeB)_{0.1}$ alloys reduces to 23.58%. Among all samples, ground particles with different shapes correspond to different phases. The major substitution occurs in $LaMg_2Ni_9$ phase. Electrochemical tests indicate that substituted alloys have different electrochemical performance, which is affected by phase structures of alloy. The discharge capacity of $La_{0.7}Mg_{0.3}Ni_3$ alloy reaches 337.3 mA·h/g, but $La_{0.7}Mg_{0.3}Ni_{2.9}(FeB)_{0.1}$ alloy gets better high rate discharge (HRD) performance at the discharge rate of 500 mA/g with a high HRD value of 73.19%.
Key words: Ni-MH battery; AB₃-type; B substitution; Co-free hydrogen storage alloy

1 Introduction

Today, batteries with high capacity and small size are demanded as mini-appliances become popular in our life. The demands of hybrid electric vehicle (HEV) and electric vehicle (EV) have promoted the research on high-capacity green power batteries. Battery materials for vehicles should have good cycling performance, high rate discharge capability and high specific discharge capacity.

Nickel/metal hydride (Ni-MH) secondary battery has been widely used due to its high energy density, high rapid charge−discharge ability and considerable safety performance. The potentially high performances of Ni-MH battery will meet the requirements of the power battery.

Hydrogen storage alloy determines the properties of the battery such as plateau potential, maximum discharge capacity, high rate discharge ability and cycling life. AB₅-type and AB₂-type hydrogen storage alloys are regular anode materials of Ni-MH batteries among hydrogen storage alloys[1]. The theoretical discharge capacity of AB₅-type alloys reaches 348 mA·h/g and that of AB₂ alloy is lower. And different methods have been studied extensively to improve the properties including element substitution[2−3]. Element Co is usually added into the alloys to make them have sufficient cycling stability and high discharge capacity. The test discharge capacity of AB₅-type alloys could reach 320−340 mA·h/g according to recent studies[4−5]. However, properties of enhanced AB₅-type alloys are still low for meeting the demands of HEV and EV. HEV and EV require a new kind of hydrogen storage alloy which has higher discharge capacity and outstanding stability under high current density.

AB₃-type hydrogen storage alloy has higher discharge capacity than AB₅-type because of the strong hydrogen storage ability of Mg element within $LaMg_2Ni_9$ phase[6−9]. According to recent studies, the discharge capacity of La-Mg-Ni AB₃-type alloys with Co element could reach 380−400 mA·h/g[10−14]. Element Co could be added into AB₃-type alloys to guarantee the cycling stability and high discharge capacity when it works in

AB$_5$-type alloys[6]. Considering that Co element is not environmentally friendly enough and can increase the cost of batteries, there are some work done on low-Co alloys in which Co was substituted by Fe or other elements[15−16]. Co-free hydrogen storage alloy has got attention and there are some studies on it in recent years[17−20].

In this work, a series of Co-free hydrogen storage alloys were directly synthesized with vacuum melting method in which Ni was substituted by Fe, B and FeB alloy, respectively. And La$_{0.7}$Mg$_{0.3}$Ni$_3$ alloy was synthesized under the same condition for comparison. The effects of B and Fe substitution on structure and electrochemical performances of hydrogen storage alloy were investigated. Morphologies and phase structure of alloy were deeply discussed, because the electrochemical performances of material mainly depend upon both morphologies and phase structure.

2 Experimental

2.1 Synthesis

La, Ni, Fe, B, MgNi$_2$ alloy and FeB alloy were used as the raw materials to synthesize the hydrogen storage alloys. The purity of La, Ni, Fe and B elements were all above 99.5% (mass fraction). MgNi$_2$ and FeB alloys were industrial products. As, La and Mg elements can easily volatilize, so 10% (mass fraction) extra amounts of them were added into raw materials, respectively. The melted alloy was cooled by water, and its oxidation layer was removed. Then, the products were manually mechanically pulverized to 50 μm. The chemical compositions of alloys were tested by inductively coupled plasma spectrometry (ICP) as shown in Table 1. The ICP results are in agreement with the target compositions.

2.2 Characterization

The XRD measurement of synthesized alloys was carried with Cu K$_\alpha$ radiation (λ=1.540 6 Å) in the scan range of 10º−100º. And the diffraction was performed with the experimental parameters of 40 kV, 150 mA and 2 (º)/min.

The ground powders were observed by SEM and carried out by EDS at the same time to characterize the particle morphologies and phase constitutions of alloys.

2.3 Electrode preparation and battery assembly

Alloy powder and carbonyl nickel (Ni-255) powder were well mixed according to 1:3 mass ratio and pressed into negative electrode disks under a pressure of 15 MPa. The industrial Ni(OH)$_2$-NiOOH positive electrode was used as the counter electrode. The working electrode and counter electrode immersed in 6 mol/L KOH alkaline solution were assembled into an open two-electrode electrolysis cell. The discharge capacities of alloys were tested by LAND test system at a current density of 150 mA/g.

2.4 Electrochemical properties characterization

The charge−discharge cycling performances of alloys were tested by the same test system at a current density of 150 mA/g and the cut-off voltage of 1 V.

High rate discharge (HRD, D) abilities of alloys were tested by following steps: open cell was activated by 3−5 charge−discharge cycles at a current density of 50 mA/g at first, then the cell was fullly charged at 50 mA/g current density. After 10 min rest, the cell was discharged at a certain current density (n) to the cut-off voltage of 1 V and the cell rested for another 10 min to dispel the polarization. The discharge capacity was recorded as C_n. After that, the cell was discharged to the cut-off voltage of 1 V at a current density of 50 mA/g and the discharge capacity was recorded as C_{50}. The D_n could be calculated by equation: $D_n(\%)=C_n/(C_n+C_{50})$.

3 Results and discussion

3.1 XRD results and analysis

The XRD patterns of melted alloys are shown in Fig.1, and cell parameters of different phases of each alloy are shown in Table 2 (the phase content are calculated by JADE software).

As shown in Fig.1, the structure of melted alloy is changed obviously due to the different substitutions. It can be seen that the La$_{0.7}$Mg$_{0.3}$Ni$_3$ alloy exhibits parts of the diffraction peaks corresponding to LaNi$_5$ phase

Table 1 Composition of melted alloys by ICP analysis

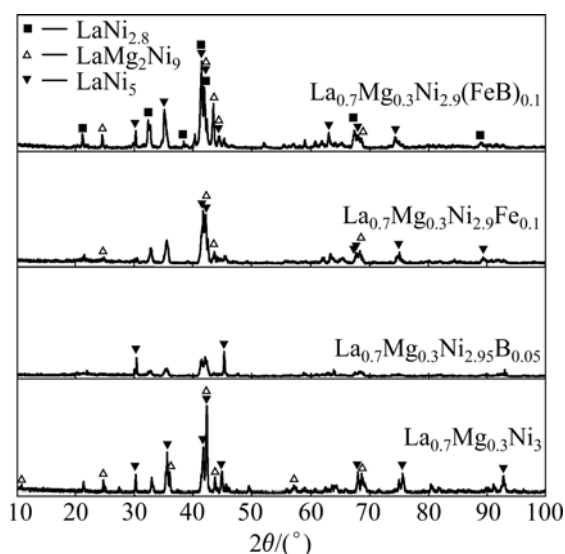| Sample	Mass fraction/%					Composition formula
	La	Mg	Ni	Fe	B	
La$_{0.7}$Mg$_{0.3}$Ni$_{2.9}$(FeB)$_{0.1}$	34.560	2.850 0	62.59	−	−	La$_{0.7}$Mg$_{0.3}$Ni$_{2.95}$B$_{0.05}$
La$_{0.7}$Mg$_{0.3}$Ni$_{2.9}$Fe$_{0.1}$	35.005	2.515 5	59.51	1.27	−	La$_{0.72}$Mg$_{0.30}$Ni$_{2.93}$Fe$_{0.07}$
La$_{0.7}$Mg$_{0.3}$Ni$_{2.9}$(FeB)$_{0.1}$	34.975	1.987 5	61.94	−	0.108 3	La$_{0.75}$Mg$_{0.26}$Ni$_{2.91}$(FeB)$_{0.09}$
La$_{0.75}$Mg$_{0.26}$Ni$_{2.91}$(FeB)$_{0.09}$	35.805	2.144 5	58.57	1.62	0.437 7	La$_{0.70}$Mg$_{0.24}$Ni$_{2.96}$B$_{0.04}$

Fig.1 XRD patterns of melted alloys and patterns of standard $LaNi_5$, $LaNi_{2.28}$ and $LaMg_2Ni_9$ phases

(JCPDF 50-0777) with the hexagonal $CaCu_5$-type structure and parts of the diffraction peaks corresponding to $LaMg_2Ni_9$ phase (JCPDF 50-1454) with hexagonal structure[9]. Calculated results in Table 2 indicate that the content of $LaNi_5$ phase reaches 62.1% in $La_{0.7}Mg_{0.3}Ni_3$ alloy, which means that the main phase of $La_{0.7}Mg_{0.3}Ni_3$ alloy is $LaNi_5$ phase. And the sharp peaks with high intensity indicate that the alloy is well crystallized. The cell parameters of $LaNi_5$ phase in melted $La_{0.7}Mg_{0.3}Ni_3$ alloy are less than those of standard $LaNi_5$ phase and this could cause difficulty of transport for H atom in alloy. The cell parameters of $LaMg_2Ni_9$ phase in melted $La_{0.7}Mg_{0.3}Ni_3$ alloy are larger than those of standard phase. There is an obvious increase in c axis length of $LaMg_2Ni_9$ phase, which could lead to the

increase in the cell volume and could have a positive effect on H atom diffusion inside alloy. And the speed of H atom diffusion inside alloy is an important property that is related to the high rate discharge performance of hydrogen storage alloys.

In contrast, alloys with substitution show less crystallization and have different phase structures from melted $La_{0.7}Mg_{0.3}Ni_3$ alloy. For $La_{0.7}Mg_{0.3}Ni_{2.9}Fe_{0.1}$ alloy, its XRD diffraction peaks become wider and weaker but remain the phases corresponding to $LaNi_5$ and $LaMg_2Ni_9$. And the main phases of $La_{0.7}Mg_{0.3}Ni_{2.9}Fe_{0.1}$ alloy are still identified to be $LaNi_5$ phase, the content of which reaches 68.9%. The cell parameters of $LaNi_5$ phase are closed to those of standard phase, and there is an increase in c axis length of $LaMg_2Ni_9$ phase as well. The XRD results of $La_{0.7}Mg_{0.3}Ni_{2.95}B_{0.05}$ alloy indicates that the substitution of Ni by non-metal element leads to very weak crystallization of hydrogen storage alloy. In $La_{0.7}Mg_{0.3}Ni_{2.95}B_{0.05}$ alloy, peaks tend to be wider and the diffraction intensity is much lower than that of other melted alloys. The results show that melted $La_{0.7}Mg_{0.3}Ni_{2.95}B_{0.05}$ alloy gets weak crystallization.

Test results indicate that melted $La_{0.7}Mg_{0.3}Ni_{2.9}$-$(FeB)_{0.1}$ alloy has more complex phase structure than other alloys. There are $LaNi_5$ phase, $LaMg_2Ni_9$ phase and $LaNi_{2.28}$ phase (JCPDF 41-0990) in the alloy when FeB alloy is added into raw materials. According to the calculation results in Table 2, the main phase of $La_{0.7}Mg_{0.3}Ni_{2.9}(FeB)_{0.1}$ alloy is $LaNi_{2.28}$ phase (phase content 48%) and parts of alloy are $LaNi_5$ phase (phase content 28.42%) and $LaMg_2Ni_7$ phase (phase content 23.58%). Although there is little increase in c axis length, the cell volume of $LaNi_{2.28}$ phase is smaller than that of standard phase due to the decrease in a axis length. Meantime, cell volumes of both $LaNi_5$ phase and

Table 2 Structure parameters of alloy phases

Sample	Type	Phase type	Phase content/%	Parameter			
				a/Å	c/Å	V/Å^3	ΔV/%
Standard $LaNi_5$ phase	−	$LaNi_5$	−	5.017 0	3.981 0	86.80	−
Standard $LaMg_2Ni_9$ phase	−	$LaMg_2Ni_9$	−	4.920 0	23.860 0	501.20	−
Standard $LaNi_{2.28}$ phase	−	$LaNi_{2.28}$	−	7.355 0	14.510 0	784.93	−
$La_{0.7}Mg_{0.3}Ni_3$	Crystal	$LaNi_5$	62.10	4.993 4	3.975 0	85.83	−1.12
		$LaMg_2Ni_9$	37.90	4.984 0	23.998 0	507.13	1.18
$La_{0.7}Mg_{0.3}Ni_{2.9}Fe_{0.1}$	Crystal	$LaNi_5$	68.90	4.994 3	3.990 4	86.20	−0.69
		$LaMg_2Ni_9$	31.10	4.939 8	23.942 0	505.96	0.95
$La_{0.7}Mg_{0.3}Ni_{2.9}(FeB)_{0.1}$	Crystal	$LaNi_5$	28.42	5.031 5	4.008 0	87.87	1.23
		$LaNi_{2.28}$	48.00	7.231 4	14.566 0	761.70	−2.96
		$LaMg_2Ni_9$	23.58	4.946 4	24.048 0	509.55	1.67

$LaMg_2Ni_9$ phase in melted $La_{0.7}Mg_{0.3}Ni_{2.9}(FeB)_{0.1}$ alloy are increased, the Δv values are 1.23% and 1.67%, respectively.

XRD results of different alloys reveal that effects of non-metal element on the structure of Co-free AB_3-type hydrogen storage alloys are different from that of common metal elements. The content of $LaMg_2Ni_9$ phase is decreased after substitution. Both B and Fe elements have a strong effect on the phase structure of hydrogen storage alloys.

3.2 SEM and EDS results

Fig.2 shows SEM images of ground particles of melted alloys. Fig.2(a) indicates that the ground particle size of $La_{0.7}Mg_{0.3}Ni_3$ alloy ranges from 1 to 30 μm, and there are both plate shape and needle shape particles. Fig.2(b) depicts that the particle size of $La_{0.7}Mg_{0.3}Ni_{2.9}(FeB)_{0.1}$ alloy ranges from 1 to 60 μm, which is larger than that of $La_{0.7}Mg_{0.3}Ni_3$ alloy. As shown in Fig.2(c), the particle size of $La_{0.7}Mg_{0.3}Ni_{2.95}B_{0.05}$ alloy ranges between 30 and 50 μm and Fig.2(d) indicates that the particle size of $La_{0.7}Mg_{0.3}Ni_{2.9}Fe_{0.1}$ alloy ranges between 5 and 50 μm. For alloys with the substitution of Fe or B element, the particles are much larger than those of non-substituted and FeB substituted alloys. In addition, particles of $La_{0.7}Mg_{0.3}Ni_{2.95}B_{0.05}$ alloy are much more homogeneous than those of other alloys.

All particles in melted alloys have sharp edge, and crystal alloys have both plate shape particles in a large scale and small granular shape particles.

EDS results were used to analyze the elements distribution in different phases of alloy as a support measures of XRD test. Although the EDS test can only provide approximate mole ratio, the main structure of alloy phases could be roughly verified according to calculated mole ratio of (Ni+Fe) to (Mg+La). The EDS test results correspond to the points shown in Fig.2, and the calculated mole ratios of alloys are shown in Table 3.

The EDS results of melted $La_{0.7}Mg_{0.3}Ni_3$ alloy correspond to two points of inserted image in Fig.2(a). EDS results corresponding to point A which represents plate shape with rough surface show an obvious spectrum of Mg element. However, the EDS results corresponding to point B which represents granular shape with smooth surface have no spectrum of Mg element. This indicates that Mg element is alternatively distributed in melted $La_{0.7}Mg_{0.3}Ni_3$ alloy and particles with different shapes have different phase structure. Calculated results in Table 3 show that the main phases of melted $La_{0.7}Mg_{0.3}Ni_3$ alloy are $LaNi_5$ phase and $LaMg_2Ni_9$ phase. This is consistent with the XRD results.

The EDS results of $La_{0.7}Mg_{0.3}Ni_{2.9}Fe_{0.1}$ alloy are similar to those of $La_{0.7}Mg_{0.3}Ni_3$ alloy, which means that Mg is alternatively distributed in $LaMg_2Ni_9$ phase. Furthermore, Fe element is alternatively distributed in different phases. And the content of deposited Fe in $LaMg_2Ni_9$ phase is more than that in $LaNi_5$ phase. This indicates that it is easier for Mg and Fe to deposit in $LaMg_2Ni_9$ phase than in $LaNi_5$ phase and the major substitution occurs in $LaMg_2Ni_9$ phase.

The EDS results of $La_{0.7}Mg_{0.3}Ni_{2.9}(FeB)_{0.1}$ alloy show that there are AB_5-type, AB_2-type and AB_3-type phases in the alloy as XRD results indicate. And these phases correspond to $LaNi_5$, $LaMg_2Ni_9$ and $LaNi_{2.28}$
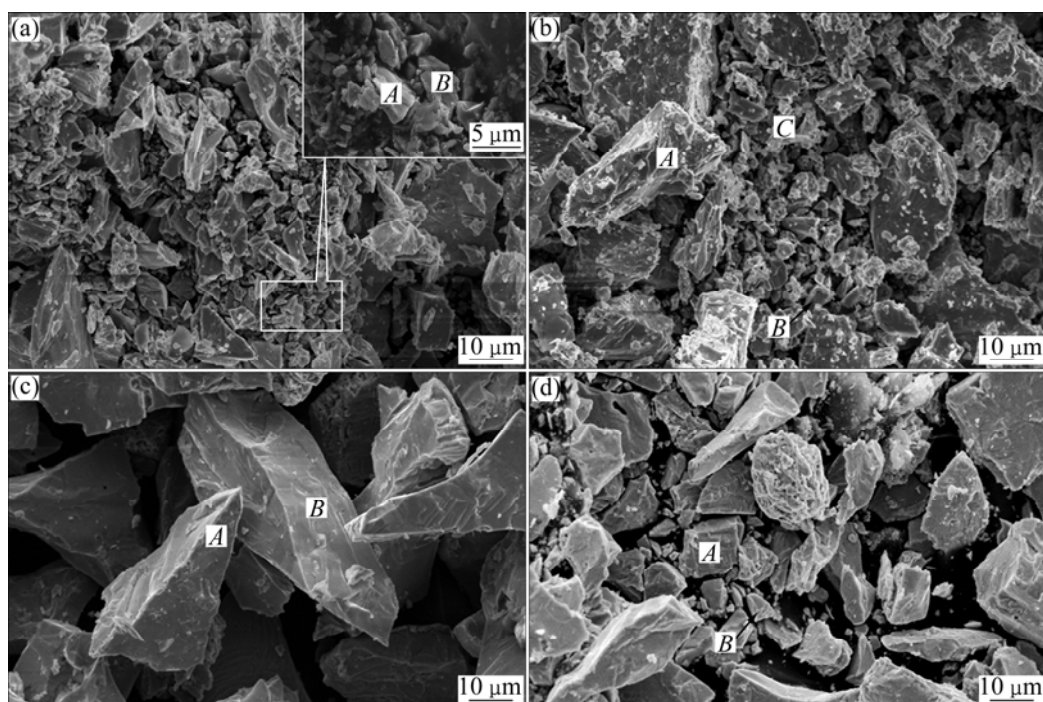

Fig.2 SEM images of $La_{0.7}Mg_{0.3}Ni_3$ (a), $La_{0.7}Mg_{0.3}Ni_{2.9}(FeB)_{0.1}$ (b), $La_{0.7}Mg_{0.3}Ni_{2.95}B_{0.05}$ (c) and $La_{0.7}Mg_{0.3}Ni_{2.9}Fe_{0.1}$ (d) alloys

Table 3 Mole ratio of points relative to SEM image in Fig.2

Sample	Point	x/%				Mole ratio of (Ni+Fe) to (Mg+La)	Corresponding phase
		Mg	Fe	Ni	La		
Melted La$_{0.7}$Mg$_{0.3}$Ni$_3$	A	9.49	−	74.87	15.24	3.027	LaMg$_2$Ni$_9$ phase
	B	0.48[1)	−	83.55	15.41	5.422	LaNi$_5$ phase
Melted La$_{0.7}$Mg$_{0.3}$Ni$_{2.9}$(Fe)$_{0.1}$	A	0.65[1)	1.73	79.63	17.98	4.525	LaNi$_5$ phase
	B	6.56	5.29	68.33	19.83	2.790	LaMg$_2$Ni$_9$ phase
Melted La$_{0.7}$Mg$_{0.3}$Ni$_{2.9}$(FeB)$_{0.1}$	A	3.69	3.10	71.95	21.26	3.026	LaMg$_2$Ni$_9$ phase
	B	1.31[1)	6.54	72.30	17.86	4.414	LaNi$_5$ phase
	C	16.58	0.22[1)	64.21	15.98	1.971	LaNi$_{2.28}$ phase
Melted La$_{0.7}$Mg$_{0.3}$Ni$_{2.95}$B$_{0.05}$	A	10.24	−	69.4	20.36	2.270	−
	B	9.30	−	68.32	22.38	2.157	−

1) Content is very low and data is inconsiderable.

phase, respectively. Mg element is alternatively distributed in LaMg$_2$Ni$_9$ phase of La$_{0.7}$Mg$_{0.3}$Ni$_{2.9}$(FeB)$_{0.1}$ alloy as well. Fe is alternatively distributed in LaMg$_2$Ni$_9$ and LaNi$_5$ phase, and the deposit contents of Fe in these two phases are 3.1% and 6.54%, respectively. The deposit content of Fe element in LaNi$_{2.28}$ phase is very low. This means that there is rare Fe substitution in LaNi$_{2.28}$ phase. Because the low boiling point of Mg, few raw material could deposit into individual fine particles during cooling procedure. The content of Mg corresponding to point C in Fig.2(d) reaches 16.58%, which may be caused by Mg element deposited into fine particle at such point.

In addition, for La$_{0.7}$Mg$_{0.3}$Ni$_{2.95}$B$_{0.05}$ alloy, the content corresponding to different points are almost the same. This means there is better elements distribution in La$_{0.7}$Mg$_{0.3}$Ni$_{2.95}$B$_{0.05}$ alloy than in others. This is probably related to the weak crystallization of phase. And the mole ratio of Ni/(Mg+La) in La$_{0.7}$Mg$_{0.3}$Ni$_{2.95}$B$_{0.05}$ alloy is less than the designed ratio, because the actual mole ratio should be calculated by (Ni+B)/(Mg+La) formula but EDS test cannot provide the valid content of B.

As the relative atom mass of B element is too light to trace, EDS results did not calculate content of B element

3.3 Discharge capacity

The cycling stability properties of synthesized alloys are shown in Fig.3. The current density in test was 150 mA/g during both charge and discharge processes. Melted alloys have different discharge performances which are related to alloy phase composition.

The discharge capacity of La$_{0.7}$Mg$_{0.3}$Ni$_3$ alloy reaches 337.3 mA·h/g, which is higher than the maximum discharge capacity of other alloys. The maximum discharge capacity of melted La$_{0.7}$Mg$_{0.3}$Ni$_{2.95}$B$_{0.05}$ alloy reaches 296.6 mA·h/g and that
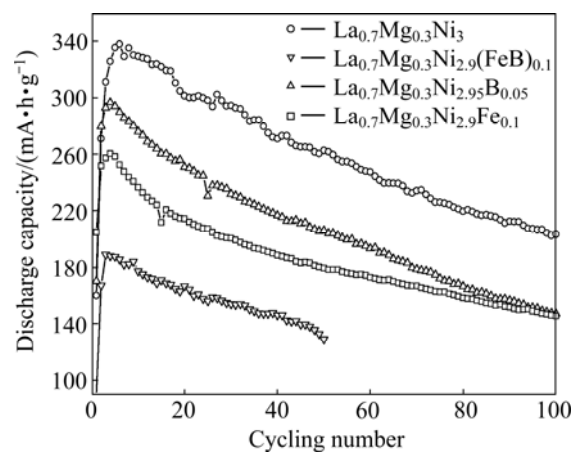

Fig.3 Discharge capacities of melted alloys at discharge current density of 150 mA/g

of La$_{0.7}$Mg$_{0.3}$Ni$_{2.9}$Fe$_{0.1}$ alloy is 260.4 mA·h/g. The discharge capacity of La$_{0.7}$Mg$_{0.3}$Ni$_{2.9}$(FeB)$_{0.1}$ alloy is 189.1 mA·h/g. This is related to LaNi$_{2.28}$ phase in the alloy because AB$_2$-type phase has much lower discharge capacity than other phases. The discharge capacity of melted alloy decreases with the decrease content of LaMg$_2$Ni$_9$ phase in different melted alloys. This indicates that LaMg$_2$Ni$_9$ phase contributes a lot to discharge capacity of hydrogen storage alloy.

The discharge curves are shown in Fig.4. Discharge plateau potentials of alloys are different. Melted La$_{0.7}$Mg$_{0.3}$Ni$_{2.95}$B$_{0.05}$ alloy has the highest plateau potential (>1.25 V) than other melted alloys. Non-substituted alloy shows a quite satisfactory discharge curve, and the plateau potential remains 1.2 V. For Fe- and FeB-substituted alloys, the plateau potentials are lower than others, which is relative to phase structure of alloys.

The performances of melted alloys under high rate discharge current density are shown in Fig.5. Test results show that as the current density increases, different alloys have obviously different discharge performance.

Melted $La_{0.7}Mg_{0.3}Ni_3$ and $La_{0.7}Mg_{0.3}Ni_{2.95}B_{0.05}$ alloy show good performance with low discharge current density. The high rate discharge ability value of $La_{0.7}Mg_{0.3}Ni_3$ alloy at the discharge rate of 150 mA/g reaches 95.3% and that of $La_{0.7}Mg_{0.3}Ni_{2.95}B_{0.05}$ alloy at the same discharge rate reaches 93.05%. However, $La_{0.7}Mg_{0.3}Ni_{2.9}(FeB)_{0.1}$ alloy shows better HRD performance at the discharge rate of 500 mA/g with a high HRD value of 73.19%. On the contrary, the HRD value of $La_{0.7}Mg_{0.3}Ni_{2.95}B_{0.05}$ alloy only remains 47.34% and that of $La_{0.7}Mg_{0.3}Ni_3$ alloy remains 58.09%. These results indicate that $La_{0.7}Mg_{0.3}Ni_{2.9}(FeB)_{0.1}$ alloy has a better discharge ability at a higher current density.
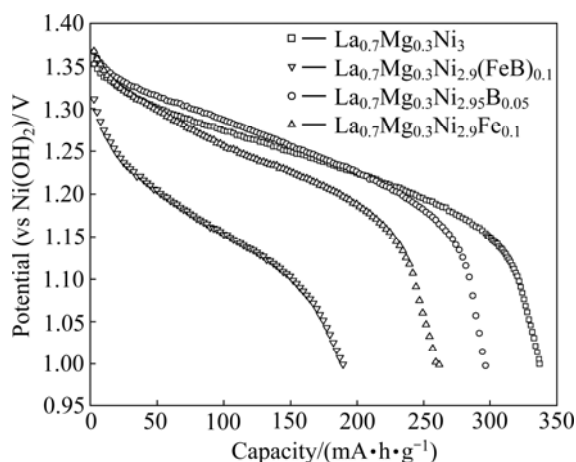

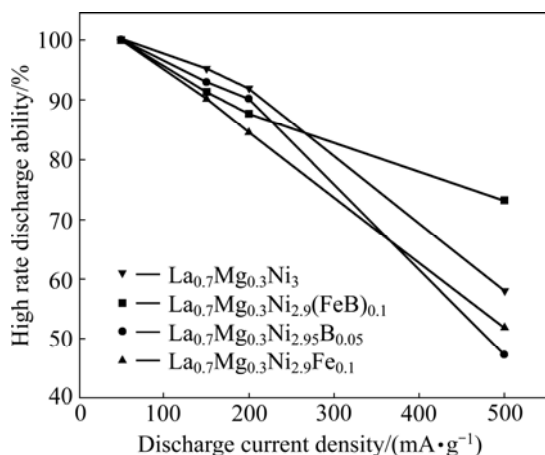**Fig.4** Discharge curves of different melted alloys at discharge current density of 150 mA/g

Fig.5 High rate discharge ability of different alloys

4 Conclusions

1) XRD results indicate that the content of different phase within melted alloy changes as the substitution element changes. The crystallization of $La_{0.7}Mg_{0.3}Ni_{2.95}B_{0.05}$ alloy is very weak. $La_{0.7}Mg_{0.3}Ni_{2.9}(FeB)_{0.1}$ alloy has a complex phase structure. The content of $LaNi_{2.28}$ phase in the alloy reaches 48% and that of $LaMg_2Ni_9$ is decreased.

2) EDS and SEM results show that alloys in which Ni is substituted by Fe element, B element and FeB alloy have different phase structures and electrochemical behaviors. Particles with different shapes correspond to different phases and both Mg and Fe elements are alternatively distributed in different phases.

3) As electrochemical properties of different phase are different, melted alloys show different electrochemical performances. The maximum discharge capacity of melted $La_{0.7}Mg_{0.3}Ni_{2.95}B_{0.05}$ alloy reaches 296.6 mA·h/g and shows a good discharge curve. The discharge capacity of $La_{0.7}Mg_{0.3}Ni_{2.9}(FeB)_{0.1}$ is relatively lower due to the low discharge capacity of $LaNi_{2.28}$ phase within hydrogen storage alloy.

4) $La_{0.7}Mg_{0.3}Ni_{2.9}(FeB)_{0.1}$ alloy shows better HRD performance than others when current density rate increases. HRD_{500} of $La_{0.7}Mg_{0.3}Ni_{2.9}(FeB)_{0.1}$ alloy reaches 73.19% while that of other alloys ranges from 45% to 60%.

References

[1]   WILLEMS J J G, BUSCHOW K H J. From permanent magnets to rechargeable hydride electrodes [J]. Journal of the Less Common Metals, 1987, 129: 13−30.

[2]   REILLY J J, ADZIC G D, JOHNSON J R, VOGT T, MUKERJEE S, MCBREEN J. The correlation between composition and electrochemical properties of metal hydride electrodes [J]. J Alloys Compd, 1987, 293: 569−582.

[3]   MNI N, RAMAPRABHU S. Effect of substitutional elements on hydrogen absorption properties in $ZrMnFe_{0.5}Ni_{0.5}$ and $ZrMnFe_{0.5}Co_{0.5}$ [J]. J Hydrogen Energy, 2005, 30(1): 53−67.

[4]   CHENG L F, WANG Y X, WANG R B, PU Z H, ZHANG X G, HE D N. Microstructure and electrochemical investigations of $La_{0.76−x}Ce_xMg_{0.24}Ni_{3.15}Co_{0.245}Al_{0.105}$ (x=0, 0.05, 0.1, 0.2, 0.3, 0.4) hydrogen storage alloys [J]. J Hydrogen Energy, 2009, 34(19): 8073−8078.

[5]   VIJAYA R, SUNDARESANA R, MAIYAB M P, SRINIVASA MURTHY S. Application of Mg-xwt% $MmNi_5$ (x=10−70) nanostructured composites in a hydrogen storage device [J]. J Hydrogen Energy, 2007, 32(13): 2390−2399.

[6]   ZHANG X B, SUN D Z, YIN W Y, CHAI Y J, ZHAO M S. Effect of La/Ce ratio on the structure and electrochemical characteristics of $La_{0.7−x}Ce_xMg_{0.3}Ni_{2.8}Co_{0.5}$ (x=0.1−0.5) hydrogen storage alloys [J]. J Electrochimica Acta, 2005, 50: 1957−1964.

[7]   LIU Yi-xin, XU Li-qin, JIANG Wei-qing, LI Guang-xu, WEI Wen-lou, GUO Jin. Effect of substituting Al for Co on the hydrogen-storage performance of $La_{0.7}Mg_{0.3}Ni_{2.6}Al_xCo_{0.5−x}$ (x=0.0−0.3) alloys [J]. J Hydrogen Energy, 2009, 34(7): 2986−2991.

[8]   QIU Shu-jun, CHU Hai-liang, ZHANG Yao, QI Yan-ni, SUN Li-xian, XU Fen. Investigation on the structure and electrochemical properties of AB_3-type La-Mg-Ni-Co-based hydrogen storage composites [J]. J Alloys Compd, 2008, 462(1/2): 392−397.

[9]   KADIR K, SAKAI T, UEHARA I. Synthesis and structure determination of a new series of hydrogen storage alloys: RMg_2Ni_9 (R=La, Ce, Pr, Nd, Sm and Gd) built from $MgNi_2$ Laves-type alternating with AB_5 layers [J]. J Alloys and Compd, 1997, 257(1/2): 115−121.

[10]   ZHANG Yang-huan, LI Bao-wei, REN Hui-ping, CAI Ying, DONG Xiao-ping, WANG Xin-lin. Investigation on structures and

electrochemical performances of the as-cast and quenched La$_{0.7}$Mg$_{0.3}$Co$_{0.45}$Ni$_{2.55-x}$Fe$_x$ (x=0−0.4) electrode alloys [J]. J Hydrogen Energy, 2007, 32(18): 4627−4634.

[11] ZHANG Yang-huan, LI Bao-wei, REN Hui-ping, WU Zhong-Wang, DONG Xiao-Ping and WANG Xin-Lin. Influences of the substitution of Fe for Ni on structures and electrochemical performances of the as-cast and quenched La$_{0.7}$Mg$_{0.3}$Co$_{0.45}$Ni$_{2.55-x}$Fe$_x$ (x=0−0.4) electrode alloys [J]. J Alloys Compd, 2008, 460(1/2): 414−420.

[12] BAI Tao-yu, HAN Shu-min, ZHU Xi-lin, ZHANG Yue, LI Yuan, ZHANG Wen-cui. Effect of duplex surface treatment on electrochemical properties of A$_B$3-type La$_{0.88}$Mg$_{0.12}$Ni$_{2.95}$Mn$_{0.10}$-Co$_{0.55}$Al$_{0.10}$ hydrogen storage alloy [J]. J Materials Chemistry and Physics, 2009, 117(1): 173−177.

[13] ZHANG Yang-huan, DONG Xiao-ping, ZHAO Dong-liang, GUO Shi-hai, QI Yan, WANG Xin-lin. Influences of stoichiometric ratio B/A on structures and electrochemical behaviors of La$_{0.75}$Mg$_{0.25}$Ni$_{3.5}$M$_x$ (M=Ni, Co; x=0−0.6) hydrogen storage alloys [J]. Transactions of Nonferrous Metals Society of China, 2008, 18(4): 857−864.

[14] LIAO B, LEI Y Q, CHEN L X, LU G L, PAN H G, WANG Q D. A study on the structure and electrochemical properties of La$_2$Mg(Ni$_{0.95}$M$_{0.05}$)$_9$ (M= Co, Mn, Fe, Al, Cu, Sn) hydrogen storage electrode alloys [J]. J Alloys and Compd, 2004, 376(1/2): 186−195.

[15] ZHANG Yang-huan, WANG Guo-qing, DONG Xiao-ping, GUO Shi-hai, REN Jiang-yuan, WANG Xin-lin. Effect of substitution Fe for Co on the cycle stability of AB$_5$-Type hydrogen storage alloys [J]. Rare Metal Materials and Engineering, 2006, 35(2): 277−282.

[16] CHENG Li-fang, WANG Run-bo, PU Chao-hui, WANG Bao-guo, LI Zhi-lin, LUO Yu-wan, HE Dan-nong, YANG Chuan-zheng. Effect of Al content on structure and electrochemical characteristics of RE$_{0.8}$Mg$_{0.2}$(Ni$_{0.85-x}$Co$_{0.15}$Al$_x$)$_{3.5}$ hydrogen storage alloys [J]. Rare Metal Materials and Engineering, 2009, 38(3), 451−455.

[17] WEI Xue-dong, ZHANG Peng, DONG Hui, LIU Yong-ning, ZHU Jie-wu, YU Guang. Electrochemical performances of a Co-free La(NiMnAlFe)$_5$ hydrogen storage alloy modified by surface coating with Cu [J]. J Alloys Compd, 2008, 458(1/2): 583−587.

[18] WEI Xue-dong, LIU She-she, DONG Hui, ZHANG Peng, LIU Yong-ning, ZHU Jie-wu, YU Guang. Microstructures and electrochemical properties of Co-free AB$_5$-type hydrogen storage alloys through substitution of Ni by Fe [J]. J Electrochimica Acta, 2007, 52(7): 2423−2428.

[19] GUO Jin, YANG Kun, XU Li-qin, LIU Yi-xin, ZHOU Kai-wen. Hydrogen storage properties of Mg$_{76}$Ti$_{12}$Fe$_{12-x}$Ni$_x$ (x=0, 4, 8, 12) alloys by mechanical alloying [J]. J Hydrogen Energy, 2007, 32(13): 2412−2416.

[20] SHAO H, ASANO K, ENOKI H, AKIBA E. Fabrication and hydrogen storage property study of nanostructured Mg-Ni-B ternary alloys [J]. J Alloys and Compd, 2009, 479(1/2): 409−413.

(Edited by LI Xiang-qun)